


Strong-coupling quantum logic of trapped ions

Mahdi Sameti, Jake Lishman , and Florian Mintert

Blackett Laboratory, Imperial College London, London SW7 2AZ, United Kingdom



(Received 16 March 2020; accepted 8 April 2021; published 11 May 2021)

Essentially all known quantum gates rely on a weak-coupling approximation resulting in linear dynamics. With the explicit example of trapped ions, we show how high-fidelity quantum gates can be achieved outside such an approximation, and we derive readily implementable driving fields to realize gates with extremely high fidelities for ions well outside the Lamb-Dicke regime with motional temperatures achievable by only Doppler cooling.

DOI: [10.1103/PhysRevA.103.052603](https://doi.org/10.1103/PhysRevA.103.052603)

I. INTRODUCTION

Entangling quantum gates are the central element in quantum information processing. After decades of experimental effort, such gates have successfully been realized in several physical systems including trapped ions [1–3], superconducting circuits [4], quantum dots [5], and NV centers [6]. After a period of proof-of-principle experiments, the field now requires fast quantum gates with extremely high fidelities for the next step towards hardware that can outperform classical devices.

Among the most advanced platforms are trapped ions [7,8]. Since ions are spatially separated due to their Coulomb repulsion, there is no appreciable direct interaction between the electronic degrees of freedom that define the qubits, and effective interactions mediated via collective motional modes need to be engineered in order to realize entangling gates. This mechanism involves a change in the motional state [9] that is absolutely essential for the implementation of the gate. It is, however, equally essential that the electronic and motional modes become uncorrelated at the gate time, as to do otherwise would result in an incoherent gate operation.

There are a variety of schemes [10–13] to drive ions with electromagnetic fields that achieve this in the *Lamb-Dicke regime* of weak ion-motion interactions with the motional modes all at low temperatures. For most of the currently employed entangling gates in the Lamb-Dicke regime, comparably simple driving schemes result in gate operations that are largely independent of the initial motional state.

Being restricted to the Lamb-Dicke regime nonetheless imposes several challenges. The necessity of keeping the ions' motion close to the quantum mechanical ground state imposes stringent requirements on cooling; only a limited number of gates can be performed between cooling cycles, which decreases the number of gates that can be executed within the coherence time. Due to the weak interactions, realizations of fast gates require strong laser driving, causing adverse effects such as AC Stark shifts and off-resonant excitations of undesired transitions, which lower the gate fidelity [14]. Even with perfectly cooled motion and weak interactions, the

Lamb-Dicke approximation still fails to be sufficient in the quest for entangling gates of ever-higher fidelity [2,3], and its corrections are now the overwhelming source of the infidelity of current quantum gates outside the weak-coupling limit [1].

Quantum gates outside this regime thus hold the potential to substantially advance the quality of quantum information processing, but existing ideas require complex sequences of intense pulses that make their experimental implementation very challenging [15,16]. The goal of this paper is thus to devise controls for entangling quantum gates beyond the Lamb-Dicke approximation that can be realized with simple driving fields.

The construction will be exemplified on the Mølmer-Sørensen gate [10,17], but applies equally to the full range of similar gates [18–20] that are currently used. The basic principle of the entangling gate can be appreciated using the level diagram in Fig. 1. In addition to carrier transitions with no change in the motional mode, there are also sideband transitions; in a k th-order red (blue) sideband transition, an excitation or deexcitation of an ion is accompanied by the annihilation or creation (creation or annihilation) of k phonons. First-order blue and red sideband transitions are depicted by solid blue and red arrows, and second-order sideband transitions are depicted by dashed arrows. The gate relies on the simultaneous driving of both the red and blue first-order sideband transitions close to, but not exactly on, resonance. Apart from the spurious excitations and deexcitations of phonons that can be made to vanish at the end of the gate operation, this results in an effective interaction between the electronic degrees of freedom, as depicted by an orange (thick) arrow in Fig. 1.

This is a truly coherent qubit-qubit interaction only under the Lamb-Dicke approximation; without it, the effective interaction strength becomes dependent on the initial state of the phonon mode and a coherent gate operation can only be ensured if this is originally a Fock state. Realistically, the motional state will be a statistical mixture of several Fock states, such as a thermal state, and the gate operation will become incoherent.

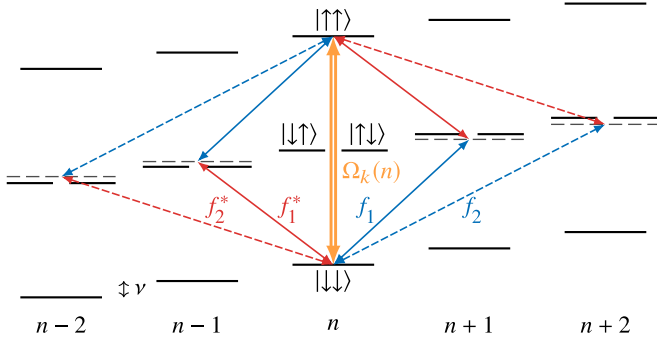


FIG. 1. Energy level diagram for two ions and one motional mode. The electronic (qubit) levels of the ions are denoted by $|\downarrow\rangle$ and $|\uparrow\rangle$, and the motional state is characterized by the phonon number n . Driving a k th-order blue and red sideband transition simultaneously close to resonance results in an effective qubit-qubit interaction with coupling constant Ω_k . Outside the Lamb-Dicke regime, this coupling depends on the phonon number n .

As will be shown here, coherent gates outside the Lamb-Dicke regime can be realized in terms of the suitable driving of higher-order sideband transitions, and the driving profiles can be obtained based on a systematic expansion in terms of the Lamb-Dicke parameter η that characterizes the coupling between electronic and motional degrees of freedom of the ions.

II. GATE DESIGN

A. Driving Hamiltonian

The starting point of the present approach is the Hamiltonian in the interaction picture for trapped ions and one motional mode driven with an external laser or microwave field with time dependence $f(t)$ that reads [18]

$$H = f(t)S_+ \exp[i\eta(ae^{-i\nu t} + a^\dagger e^{i\nu t})] + \text{H.c.}, \quad (1)$$

where ν is the frequency of the motional mode; the Lamb-Dicke parameter η is given by the ratio of the photon momentum of the driving field to the phonon momentum of the motional mode; $S_\pm = \sum_j \sigma_\pm^{(j)}$ are the collective qubit raising and lowering operators; and a (a^\dagger) are the phonon annihilation (creation) operators.

All the previously mentioned complications arising outside the Lamb-Dicke regime result from the nonlinear dependence of H on the phonon creation and annihilation operators. In order to appreciate this, it is instructive to express the exponential function in Eq. (1) as

$$\exp[i\eta(ae^{-i\nu t} + a^\dagger e^{i\nu t})] = e^{-\eta^2/2} \sum_{k=-\infty}^{\infty} \mathcal{D}_k(\eta) e^{ik\nu t}, \quad (2)$$

with

$$\mathcal{D}_k(\eta) = \sum_{n=0}^{\infty} (i\eta)^{2n+k} \frac{a^{\dagger n+k}}{(n+k)!} \frac{a^n}{n!} \quad \text{for } k \geq 0, \quad (3)$$

and $\mathcal{D}_{-k}(\eta) = \mathcal{D}_k^\dagger(-\eta)$. The term \mathcal{D}_0 corresponds to carrier transitions since it preserves the phonon number, and the terms \mathcal{D}_k with $k > 0$ and $k < 0$ correspond to blue and red

sideband transitions of order k , respectively. In the frequently employed Lamb-Dicke approximation, the sum in Eq. (3) is restricted to terms that are, at most, first order in η , resulting in a linear Hamiltonian corresponding to linear Heisenberg equations of motion. In general, however, the qubit-phonon coupling is nonlinear, as reflected by Eq. (3).

Most entangling gates are realized in terms of a two-photon process comprised of a transition of both the first-order red and blue sidebands, with effective coupling constant

$$\Omega_1 \propto [\mathcal{D}_1(\eta), \mathcal{D}_{-1}(\eta)] = \eta^2 - 2\eta^4 a^\dagger a + O(\eta^6) \quad (4)$$

for the entangling qubit-qubit interaction. In lowest order ($\propto \eta^2$), this is indeed independent of the initial phonon occupation, whereas the dependence on $a^\dagger a$ at fourth and higher orders modifies the effective process from a coherent interaction between two qubits to a three-body interaction between two qubits and the motional mode.

Driving additional blue and red sidebands of the same order simultaneously engenders complementary resonant two-photon processes, which contribute additional terms $\Omega_k \propto [\mathcal{D}_k, \mathcal{D}_{-k}]$ for $k > 1$ to the coupling constant. The goal of the present approach is to combine simultaneous driving of sufficiently many higher-order sidebands with appropriate fields such that the phonon-number-dependent processes cancel.

To achieve this, we consider driving protocols with the generic temporal pattern

$$f(t) = -i \frac{e^{\eta^2/2}}{\eta} \sum_{k>0} [f_k(t) e^{-ik\nu t} + (-1)^k f_k^*(t) e^{ik\nu t}]. \quad (5)$$

The first (second) term in this ansatz corresponds to the driving of the k th-order blue (red) sidebands, and the factors $f_k(t)$ vary slowly in time to ensure that this driving is slightly off-resonant. The phase factor $(-1)^k$ and the prefactor $e^{\eta^2/2}\eta^{-1}$ can be understood as a convention that can be chosen at will, as long as the factors $f_k(t)$ are not determined yet. This particular choice of phase factors will result in a more systematic expansion later on, and the factor $e^{\eta^2/2}$ is chosen to cancel the first factor in Eq. (2). While these choices are mostly for convenience, the prefactor η^{-1} is essential for the expansion in powers of η and it reflects the fact that a decreasing Lamb-Dicke parameter requires increasing amplitudes of the driving fields in order to maintain a constant entangling interaction.

Neglecting far-off-resonant processes in the interaction Hamiltonian of Eq. (1) with the explicit driving profile in Eq. (5) results in the compact Hamiltonian

$$H_s = \frac{1}{\eta} S_y \sum_k [f_k(t) \mathcal{D}_k(\eta) + f_k^*(t) \mathcal{D}_k^\dagger(\eta)]. \quad (6)$$

B. Solving nonlinear dynamics

Inside the Lamb-Dicke regime, this reduces to the linear Mølmer-Sørensen Hamiltonian $H_0 = iS_y(f_1 a^\dagger - f_1^* a)$, for which the time evolution is given by

$$\mathcal{U}_0(t) = \exp[S_y(\{f_1\}a^\dagger - \{f_1^*\}a) + i\Phi_0 S_y^2]. \quad (7)$$

The lowest-order Rabi angle $\Phi_0(t) = \text{Im} \{f_1\{f_1^*\}\}$ is specified in terms of the shorthand notation $\{f\} = \int_0^t dt_1 f(t_1)$ and its nesting $\{f\{g\}\} = \int_0^t dt_1 f(t_1) \int_0^{t_1} dt_2 g(t_2)$.

In order to solve the system dynamics outside the Lamb-Dicke regime including terms up to a high order in η , the exact propagator \mathcal{U} is approximated by a product \mathcal{V}_d of time-dependent unitaries \mathcal{U}_j as

$$\mathcal{U} \approx \mathcal{V}_d = \mathcal{U}_0 \mathcal{U}_1 \cdots \mathcal{U}_{d-1} \mathcal{U}_d. \quad (8)$$

This product is constructed such that the generator of \mathcal{U}_j is proportional to η^j , except for the final factor \mathcal{U}_d which contains terms of order η^d and higher. The starting unitary \mathcal{U}_0 is defined as the solution to the linearized Hamiltonian to coincide with Eq. (7). Successive time-dependent unitaries \mathcal{U}_j are defined by considering transformed Hamiltonians,

$$H_{j+1} = \mathcal{V}_j^\dagger H_s \mathcal{V}_j - i \mathcal{V}_j^\dagger \dot{\mathcal{V}}_j, \quad (9)$$

that contain only terms of order at least η^{j+1} . With the solution of the linearized problem \mathcal{U}_0 , this is naturally ensured for H_1 . Denoting the terms in leading order of η of H_j by \bar{H}_j , i.e., $\bar{H}_j \propto \eta^j$, one can define the propagator $\mathcal{U}_1 = \exp(-i\{\bar{H}_1\})$. Since \mathcal{U}_1 solves the Schrödinger equation with Hamiltonian H_1 in leading order of η , H_2 is of the order of at least η^2 . This process can be iterated by defining the unitary \mathcal{U}_j entering Eq. (8) as $\mathcal{U}_j(t) = \exp(-i\{\bar{H}_j\})$. This definition ensures that the subsequent Hamiltonian H_{j+1} defined in Eq. (9) contains only terms of the order of at least η^{j+1} .

These ensuing Hamiltonians are nonterminating; however, the Baker-Campbell-Hausdorff expansion permits a series expansion in ascending powers of η . Under the frame transformations of Eq. (9), the next Hamiltonian is a sum over nested commutators,

$$H_{j+1} = \sum_{m=1}^{\infty} \underbrace{\left[i\{\bar{H}_j\}, \cdots \left[i\{\bar{H}_j\}, H_j - \frac{1}{m} \bar{H}_j \right] \cdots \right]}_{(m-1) \text{ commutators}}, \quad (10)$$

such that each element of the sum contains only terms of higher order than η^{mj} .

After d steps, one arrives at a Hamiltonian $H_d \sim \eta^d$ which still permits an exact solution to the Schrödinger equation, but at this step it is approximated by $\mathcal{U}_d = \exp(-i\{H_d\})$, where, in contrast to the previous steps, this construction is not limited to the dominant part of H_d . This approximate propagator differs from the exact propagator by terms of order at least η^{2d} since the lowest-order terms that are being neglected are bilinear in H_d .

The desired entangling interaction S_y^2 is contained in \mathcal{U}_0 in Eq. (7). In addition to that, \mathcal{U}_0 also contains terms proportional to aS_y and $a^\dagger S_y$, corresponding to the annihilation and creation of a phonon conditioned on the state of the qubits. A perfectly coherent gate in lowest order in η is thus realized if $\{f_1\}$ vanishes at the gate time T , and if $\Phi_0(T)$ coincides with the desired Rabi angle Φ_T . In order to realize a coherent gate to higher order in η , it is necessary to ensure that the additional factors $\mathcal{U}_j(T)$ in Eq. (8) reduce to the identity or contribute solely to the coherent interaction between the qubits. For general driving patterns, however, the factors \mathcal{U}_j contain processes of the form $a^{\dagger p} a^q S_y^r$ with scalar prefactors depending

on the driving profiles f_k . The requirement that each of these prefactors must vanish at $t = T$ defines a constraint that the driving profiles must satisfy. Since the derivation of each constraint follows exactly the same pattern, we will sketch it here with the process $a^\dagger a S_y^2$ in \mathcal{U}_2 as an illustrative example. The corresponding prefactor is $\eta^2 (\frac{1}{2} \{f_2\{f_2^*\} - f_2^* \{f_2\}\} - 2i\Phi_0)$. The requirement that the process $a^\dagger a S_y^2$ must not contribute to the gate thus results in the constraint $\text{Im} \{f_2\{f_2^*\}\} = 2\Phi_0(T)$ at the gate time. In a similar fashion, all processes contributing to the full propagator $\mathcal{V}_d(T)$ to any desired order d can be taken into account. See the Appendix for a full reproduction of all conditions at third order, and the attached data repository for computer-readable representations of all conditions at both third and fourth orders, and Python code to generate the conditions at arbitrary order [28].

III. EXAMPLE GATES

These constraints are satisfied for a broad range of driving profiles that can be selected depending on experimental constraints, goals, and capabilities. In the following, we will discuss two such profiles that solve the conditions to third and fourth orders, that is considering terms up to and including η^3 or η^4 . To third order, only two sidebands are necessary, each driven monochromatically close to resonance with $f_1(t) = \Omega \exp(2i\delta t)$ and $f_2(t) = \Omega \exp(i\delta t)$ for a gate time of $T = 2\pi/\delta$, with Ω determined by the entangling condition on the Rabi angle. For this specific driving profile, this condition is $3\eta^2 x^4 - (1 + \eta^2)x^2 + \Phi_T/\pi = 0$, with $x = \Omega/\delta$, and the following discussion is based on the smallest positive root of this equation to minimize power usage.

The extension to fourth order requires driving the third sideband, and the driving profiles

$$f_1(t) = \Omega \exp(5i\delta t), \quad f_3(t) = \sqrt{\frac{3}{5}} \Omega \exp(i\delta t), \quad (11)$$

$$f_2(t) = \frac{\Omega}{\sqrt{5}} \left[2 \exp(2i\delta t) + \frac{7}{5} \frac{\Omega}{\delta} \eta \exp(-7i\delta t) \right], \quad (12)$$

with bichromatic driving of the second sideband, are a valid solution to all constraints, with Ω determined by

$$\frac{382}{1875} x^6 - \frac{56}{75} \left(2 + \frac{1}{\eta^2} \right) x^4 + \left(1 + \frac{2}{\eta^2} + \frac{2}{\eta^4} \right) x^2 = \frac{5}{\pi \eta^4} \Phi_T. \quad (13)$$

The gate infidelity is strongly dependent on both the Lamb-Dicke parameter and the initial motional excitation. It is plotted for a fixed gate time $T = 2\pi/\delta$ and Rabi angle $\Phi_T = \pi/8$ corresponding to the creation of a Bell state as a function of the Lamb-Dicke parameter in Fig. 2(a) for the three schemes under discussion, with different starting motional Fock states. The solutions have the dependences $\sim \eta^4$, $\sim \eta^8$, and $\sim \eta^{10}$ that are consistent with the perturbative construction of the driving patterns. In Figs. 2(b)–2(d), this infidelity is plotted for each scheme, respectively, for the motion in an initial thermal state with varying mean occupation. Extremely high fidelities can be reached for a broad range of Lamb-Dicke parameters in Figs. 2(c) and 2(d), whereas the conventional driving depicted in Fig. 2(b) requires a small value of the

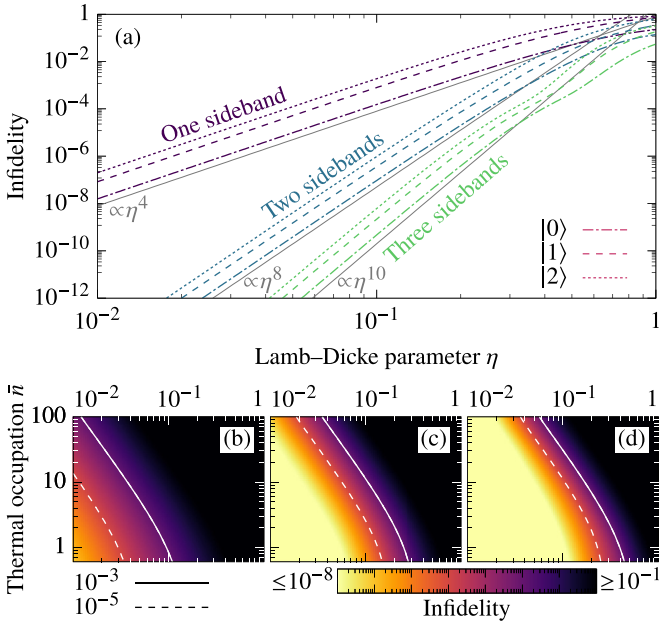


FIG. 2. (a) Gate infidelity as a function of Lamb-Dicke parameter η for the schemes with one (purple, dark), two (blue, middle), and three (green, light) sidebands, starting from motional pure states $|0\rangle$ (dot-dashed), $|1\rangle$ (dashed), and $|2\rangle$ (dotted). The present driving reduces the dependence of η from $O(\eta^4)$ for the standard gate to $O(\eta^8)$ and $O(\eta^{10})$ for the two- and three-sideband gates, respectively. Lines with the exact power laws are shown in solid gray for comparison. (b)–(d) Heat maps of the infidelity for a motional thermal state with varying mean occupation \bar{n} for different values of η , using a scheme with (b) one, (c) two, and (d) three sidebands. Contours are plotted at infidelities of 10^{-3} (solid) and 10^{-5} (dashed).

Lamb-Dicke parameter and a low motional temperature for a good gate fidelity.

Previous experimental work seeking fast gates has used a Lamb-Dicke parameter of approximately 0.1 with the average motional excitation cooled to $\bar{n} \lesssim 0.05$ [1]. At this level, outside-Lamb-Dicke effects lower-bound the single-sideband gate infidelity to 1.9×10^{-4} , whereas the additions of second and third sidebands reduce the bound to 1.1×10^{-7} and 7×10^{-10} , respectively. The same fidelity as the base gate can be achieved by the second-order (third-order) scheme with a Lamb-Dicke parameter up to 0.27 (0.43) or a thermal state with average occupation $\bar{n} \leq 6.6$ (21). That is, the present driving schemes would allow the realization of gates with state-of-the-art fidelities even without sideband cooling, and since all driving frequencies are spectrally close to the qubit transition frequency, both schemes can readily be realized with standard pulse-shaping equipment.

The improvements in infidelities of these two particular driving schemes over the base gate can be better understood through consideration of the phase-space displacement of the motional mode during the gate operation. Figure 3 depicts this for an initial state with the qubits in an eigenstate of S_y and the motion in a thermal state, for conditions both inside (top) and outside (bottom) the Lamb-Dicke regime. The left

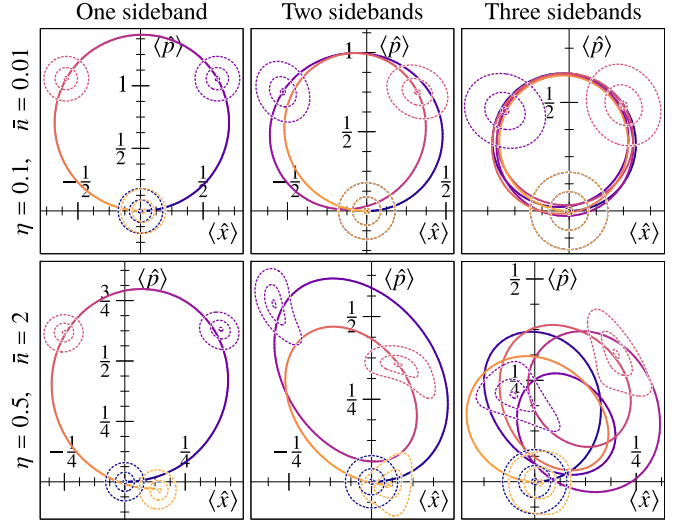


FIG. 3. Phase-space trajectories of gates using one, two, and three sidebands (columns), both inside the Lamb-Dicke regime (top row) and far outside (bottom row). Contours of the Wigner function of the motional state at times 0, $T/3$, $2T/3$, and T are indicated by the dashed lines, scaled down around their centroids to 25% (top) or 5% (bottom) for visibility. Time through gate is represented by the color, ranging from purple (dark) to orange (light). A high-fidelity gate is realized only if the initial and final Wigner functions coincide. Outside the Lamb-Dicke regime, increased contributions from the higher-order sidebands modify the phase-space trajectories and cause substantial deformation of the Wigner functions. With conventional driving (one sideband), there is thus a substantial deviation between the initial and final states. With two sidebands, or even more with three, however, the phase-space trajectory closes rather accurately, and the distortion of the Wigner function vanishes to a good approximation at the end of the dynamics.

column illustrates the dynamics resulting from conventional driving of only first-order sidebands, while the central and right columns correspond to third- and fourth-order cases. Outside the Lamb-Dicke regime, the phase-space trajectory (i.e., the expectation of position and momentum) does not form a closed loop with the conventional driving scheme, whereas the trajectories in the other two cases close nearly perfectly, as required for coherent quantum gates.

In addition to the phase-space trajectory, a scaled-down version of the Wigner function is depicted at thirds of the gate time with dashed contour lines. With conventional driving (left), the contour shapes hardly change, but the present driving schemes result in strong deformations. This is direct evidence of the exploitation of the second- and third-order sideband transitions, and it is exactly those nonlinear processes that manage to correct the phase-space trajectory. Since the Wigner function and phase-space trajectory are not drawn to the same scale, the overlap between initial (orange, light) and final (purple, dark) Wigner functions is substantially larger than suggested by the figure. While the figure therefore cannot offer a quantitative estimate of this overlap, one can see that it becomes larger from left to right as expected, and the corresponding gate fidelities are 71%, 89%, and 97.3%.

IV. DISCUSSION

The technique developed here allows for precise control of the trapped-ion system in the nonlinear regime, which has remained inaccessible so far. The linear approximation imposes a fundamental limit on the achievable fidelity in state-of-the-art trapped-ion quantum gates, which cannot be exceeded by improvement of the experimental control apparatus. The present systematic method removes this limit by canceling the undesired contributions originating from the nonlinear nature of the interaction order by order. Even under unfavorable experimental conditions such as imperfect cooling, this scheme leads to extremely high fidelity of quantum operations. This work opens avenues to high-temperature quantum information processing with trapped ions, removing the need for expensive sideband-cooling cycles.

The generic method introduced here leads to a set of functional constraints for a suitable driving ansatz. The two explicitly given solutions illustrate the efficient performance of the proposed technique with experimentally standard pulses even for large values of the Lamb-Dicke parameter. However, the framework admits a broad spectrum of different solutions that can accommodate the advantages of other current proposals as well. The sidebands may, for example, be driven polychromatically or with phase modulation to achieve additional robustness against heating and uncertainty in driving parameters [21–24]. The techniques developed here thus should not be seen as an alternative to existing control techniques, but rather as a seamless addition to the existing ion-trapping toolbox [19,20,25]. This paper mainly focused on canceling adverse effects of the strong-coupling limit of a nonlinear interaction; however, the strategy can equally be employed to exploit advantages of

this regime, for example to implement fast or multiqubit gates.

More broadly, the proposed approach is a powerful tool to devise driving protocols starting from a variety of initial Hamiltonians; the general framework is exemplified here for the Mølmer-Sørensen scheme, but readily applies to any quantum gate that is based on a linearized interaction. It is thus by no means limited to trapped ions, and can find application in any system for which fundamentally nonlinear interactions are approximated to their leading order. One prominent example is given by superconducting qubits [26], which are two-level approximations of anharmonic oscillators, and leakage out of the qubit subspace poses severe restrictions on achievable fidelities.

Similarly, the interactions between light and mechanical oscillators in cavity optomechanics [27] are fundamentally nonlinear; they can be approximated as linear under strong driving, with nonlinearities becoming more relevant with decreasing driving amplitude. As it enables control over a broad range of nonlinearities, the present framework is not limited to the realization of quantum gates, but can also be applied for the design of high-precision sensors or other quantum-technological devices.

ACKNOWLEDGMENTS

We are grateful for stimulating discussions with Joe Goodwin, Oliver Corfield, Richard Thompson, and Simon Webster. Financial support by Engineering and Physical Sciences Research Council (EPSRC) through the Optimal control for robust ion trap quantum logic Grant No. EP/P024890/1 and the Training and Skills Hub in Quantum Systems Engineering Grant No. EP/P510257/1 is gratefully acknowledged.

APPENDIX: EXPLICIT FUNCTIONAL CONDITIONS FOR THIRD ORDER

The desired entangling interaction that is accurate up to and including terms of order η^3 can be realized by driving only two sidebands with amplitudes f_1 and f_2 . In order to ease notation, the conditions that need to be satisfied are expressed in terms of the shorthand notations

$$\{f\} = \int_0^t dt_1 f(t_1), \quad (\text{A1})$$

where nesting implies iteration of the integration, i.e.,

$$\{f_1\{f_2\}\} = \int_0^t dt_1 f_1(t_1) \int_0^{t_1} dt_2 f_2(t_2) \quad (\text{A2})$$

and so on, and

$$\lambda(x, y) = x\{y\} - y\{x\}. \quad (\text{A3})$$

The entangling condition at the gate time $t = T$ is

$$\Phi_T = \text{Im} \left\{ f_1\{f_1^*\} + \frac{1}{2}\eta^2 f_2\{f_2^*\} - 4\eta^2\{f_1\}(f_2^*\{f_1^*\}f_2) + f_1\{f_1^{*2}\} \right\}. \quad (\text{A4})$$

In addition to Eq. (A4), all the following quantities also need to vanish at $t = T$:

$$\{f_1\}; \quad \{f_2\}; \quad \{f_1\}f_2^*; \quad \{f_1\{f_1\}\}; \quad (\text{A5})$$

$$\{f_1\{f_2^*\}\}; \quad \text{Re} \{ \{f_1\}\{f_1\}f_2^* \}; \quad \{3f_1\{f_2\} + \{f_1\}f_2\}; \quad (\text{A6})$$

$$\left\{ \{f_1^*\} (2f_1^* \{f_1\} + f_2 \{f_2^*\} - f_1 \{f_1^*\}) - f_2^* \{ \{f_1^*\} f_2 \} \right\}; \quad (\text{A7})$$

$$\left\{ 2\{f_2\} [3\lambda(f_1, f_1^*) - \lambda(f_2, f_2^*)] + 3f_1 \{ \{f_1^*\} f_2 \} + 3\{f_1\} \{f_1^*\} f_2 \right\}; \quad (\text{A8})$$

$$\left\{ 12\{f_1^*\} \text{Re} [f_1 \{ \{f_1\} \{f_2^*\} \}] + 6f_1 \{f_1\} \{f_1^*\} \{f_2^*\} - 4f_2 \{f_2^*\} \{ \{f_1\} f_2^* \} - 3\{f_1\}^2 (\{f_1^*\} f_2^* + f_1^* \{f_2^*\}) \right\} \\ + \left\{ 2\{f_1\} f_2^* \{f_2\} \{f_2^*\} - \{f_1^*\}^3 \{f_2\} - 2\{ \{f_1\} f_2^* \} (3f_1^* \{f_1\} - f_2^* \{f_2\}) \right\}; \quad (\text{A9})$$

$$\text{Re} \left\{ 4\{ \{f_1\} f_2^* \} \left[\{f_1\} (6f_1 \{f_1^*\} - 3f_1^* \{f_1\} + 2f_2^* \{f_2\}) - 2f_2 \{ \{f_1\} f_2^* \} \right] - 4\{f_1\}^3 \{f_1^*\} f_2^* + 3f_1 \{f_1\} \{f_2^*\} \right\}; \quad (\text{A10})$$

$$\{2\lambda(f_1, f_1^*) - \lambda(f_2, f_2^*)\}. \quad (\text{A11})$$

All quantities listed in Eqs. (A5) to (A10) are satisfied by the driving fields specified in the main article because they are monochromatic with frequencies given by δ and 2δ . Equation (A11) is satisfied because, in addition to this, $f_1(t)$ and $f_2(t)$ have the same magnitude.

-
- [1] V. M. Schäfer, C. J. Ballance, K. Thirumalai, L. J. Stephenson, T. G. Ballance, A. M. Steane, and D. M. Lucas, Fast quantum logic gates with trapped-ion qubits, *Nature (London)* **555**, 75 (2018).
 - [2] T. P. Harty, M. A. Sepiol, D. T. C. Allcock, C. J. Ballance, J. E. Tarlton, and D. M. Lucas, High-Fidelity Trapped-Ion Quantum Logic Using Near-Field Microwaves, *Phys. Rev. Lett.* **117**, 140501 (2016).
 - [3] J. P. Gaebler, T. R. Tan, Y. Lin, Y. Wan, R. Bowler, A. C. Keith, S. Glancy, K. Coakley, E. Knill, D. Leibfried, and D. J. Wineland, High-Fidelity Universal Gate Set For $^9\text{Be}^+$ Ion Qubits, *Phys. Rev. Lett.* **117**, 060505 (2016).
 - [4] M. Reagor *et al.*, Demonstration of universal parametric entangling gates on a multi-qubit lattice, *Sci. Adv.* **4**, eaao3603 (2018).
 - [5] M. Veldhorst *et al.*, A two-qubit logic gate in silicon, *Nature (London)* **526**, 410 (2015).
 - [6] X. Rong, J. Geng, F. Shi, Y. Liu, K. Xu, W. Ma, F. Kong, Z. Jiang, Y. Wu, and J. Du, Experimental fault-tolerant universal quantum gates with solid-state spins under ambient conditions, *Nat. Commun.* **6**, 8748 (2015).
 - [7] A. Bermudez, X. Xu, R. Nigmatullin, J. O’Gorman, V. Negnevitsky, P. Schindler, T. Monz, U. G. Poschinger, C. Hempel, J. Home, F. Schmidt-Kaler, M. Biercuk, R. Blatt, S. Benjamin, and M. Müller, Assessing The Progress Of Trapped-Ion Processors Towards Fault-Tolerant Quantum Computation, *Phys. Rev. X* **7**, 041061 (2017).
 - [8] C. D. Bruzewicz, J. Chiaverini, R. McConnell, and J. M. Sage, Trapped-ion quantum computing: Progress and challenges, *Appl. Phys. Rev.* **6**, 021314 (2019).
 - [9] D. Leibfried, R. Blatt, C. Monroe, and D. Wineland, Quantum dynamics of single trapped ions, *Rev. Mod. Phys.* **75**, 281 (2003).
 - [10] A. Sørensen and K. Mølmer, Entanglement and quantum computation with ions in thermal motion, *Phys. Rev. A* **62**, 022311 (2000).
 - [11] J. J. García-Ripoll, P. Zoller, and J. I. Cirac, Coherent control of trapped ions using off-resonant lasers, *Phys. Rev. A* **71**, 062309 (2005).
 - [12] C. Ospelkaus, C. E. Langer, J. M. Amini, K. R. Brown, D. Leibfried, and D. J. Wineland, Trapped-Ion Quantum Logic Gates Based on Oscillating Magnetic Fields, *Phys. Rev. Lett.* **101**, 090502 (2008).
 - [13] A. Bermudez, P. O. Schmidt, M. B. Plenio, and A. Retzker, Robust trapped-ion quantum logic gates by continuous dynamical decoupling, *Phys. Rev. A* **85**, 040302(R) (2012).
 - [14] A. Steane, C. F. Roos, D. Stevens, A. Mundt, D. Leibfried, F. Schmidt-Kaler, and R. Blatt, Speed of ion-trap quantum-information processors, *Phys. Rev. A* **62**, 042305 (2000).
 - [15] J. Mizrahi, B. Neyenhuis, K. G. Johnson, W. C. Campbell, C. Senko, D. Hayes, and C. Monroe, Quantum control of qubits and atomic motion using ultrafast laser pulses, *Appl. Phys. B* **114**, 45 (2014).
 - [16] J. D. Wong-Campos, S. A. Moses, K. G. Johnson, and C. Monroe, Demonstration of Two-Atom Entanglement With Ultrafast Optical Pulses, *Phys. Rev. Lett.* **119**, 230501 (2017).
 - [17] A. Sørensen and K. Mølmer, Quantum Computation With Ions in Thermal Motion, *Phys. Rev. Lett.* **82**, 1971 (1999).
 - [18] C. F. Roos, Ion trap quantum gates with amplitude-modulated laser beams, *New J. Phys.* **10**, 013002 (2008).
 - [19] S. Weidt, J. Randall, S. C. Webster, K. Lake, A. E. Webb, I. Cohen, T. Navickas, B. Lekitsch, A. Retzker, and W. K. Hensinger, Trapped-Ion Quantum Logic With Global Radiation Fields, *Phys. Rev. Lett.* **117**, 220501 (2016).
 - [20] T. Choi, S. Debnath, T. A. Manning, C. Figgatt, Z.-X. Gong, L.-M. Duan, and C. Monroe, Optimal Quantum Control Of Multimode Couplings Between Trapped Ion Qubits For Scalable Entanglement, *Phys. Rev. Lett.* **112**, 190502 (2014).
 - [21] F. Haddadfarshi and F. Mintert, High fidelity quantum gates of trapped ions in the presence of motional heating, *New J. Phys.* **18**, 123007 (2016).
 - [22] A. E. Webb, S. C. Webster, S. Collingbourne, D. Breaud, A. M. Lawrence, S. Weidt, F. Mintert, and W. K. Hensinger, Resilient Entangling Gates for Trapped Ions, *Phys. Rev. Lett.* **121**, 180501 (2018).
 - [23] Y. Shapira, R. Shaniv, T. Manovitz, N. Akerman, and R. Ozeri, Robust Entanglement Gates for Trapped-Ion Qubits, *Phys. Rev. Lett.* **121**, 180502 (2018).

- [24] A. R. Milne, C. L. Edmunds, C. Hempel, F. Roy, S. Mavadia, and M. J. Biercuk, Phase-Modulated Entangling Gates Robust to Static and Time-Varying Errors, *Phys. Rev. Appl.* **13**, 024022 (2020).
- [25] M. Palmero, S. Martínez-Garaot, D. Leibfried, D. J. Wineland, and J. G. Muga, Fast phase gates with trapped ions, *Phys. Rev. A* **95**, 022328 (2017).
- [26] G. Wendin, Quantum information processing with superconducting circuits: A review, *Rep. Prog. Phys.* **80**, 106001 (2017).
- [27] M. Aspelmeyer, T. J. Kippenberg, and F. Marquardt, Cavity optomechanics, *Rev. Mod. Phys.* **86**, 1391 (2014).
- [28] <https://github.com/ImperialCQD/Strong-Coupling-Quantum-Logic-of-Trapped-Ions>.